Deciphering Short-Range Order Driven Mechanical Enhancement in CrTaTiMo Refractory Alloys via Machine-Learning Potential and Experimental Validation

Supplementary Information

Xiao Wang[a], Arman Hobhaydar[a], Huijun Li[a], Lihong Su[a], Sam Moricca[c], Nam Van Tran[b*], Hongtao Zhu[a*]

[a] School of Mechanical, Materials, Mechatronic and Biomedical Engineering, University of Wollongong, Northfields Avenue, Wollongong, NSW 2522, Australia.

[b] School of Materials Science and Engineering, Nanyang Technological University, 50 Nanyang Avenue, Singapore 639798.

[c] Gravitas Technologies, 14 John Cleary Place, Coniston NSW 2500, Australia

* Email: vannam.tran@ntu.edu.sg

* Email: hongtao@uow.edu.au

1 Additional information for Methods

1.1 Machine-learning Potential Training

The main idea of the DP method is described in **Equation S1**. The local environment of centric atoms is described as a matrix. R_i, which contain the distance information between centric atoms and neighbours. Then, by embedding the distance information (R_i) into a matrix G and matrix multiplication, a descriptor vector, D_{a_i}, can be extracted. Moreover, a deep neural network, N_{a_i} is used to approximate the contribution of each atom's information to the energy, to obtain the total energy of the system.

$$E = \sum_i N_{a_i}(D_{a_i}(r_i, \{r_j\}_{j\in n(i)})) \qquad \textbf{Equation S1}$$

To facilitate an effective machine learning process, the DPGEN package enables a sequence of successive training iterations involving training, exploration, and labelling. Firstly, an initial DFT dataset is constructed to provide a reliable initial guess for the deep neural network. Subsequently, the iteration for potential training begins. In each iteration, the dataset is used in the deep neural network to train DP interatomic potentials. The four trained potentials are then utilised in long-time MD simulations under various conditions to explore configurational space. Among these configurations, candidates that satisfy the error criteria are labelled. The candidate configurations undergo DFT calculations to obtain accurate energy and force information, which are then added to the dataset to augment it and improve the DP model. The training iteration will finish when the convergence criteria are met.

1.2 Exploration of Training Dataset

The initial dataset consisted of 10-step AIMD calculations using the *init* function in DPGEN and long-time AIMD calculations. Bellowing structures were included in the initial dataset: an equimolar BCC CrTaTiMo RMEA 128-atom structure, pure elements include BCC Cr, BCC Ta, BCC Mo, BCC Ti 128-atom structure, as well as HCP Ti 96-atom structure, and Cr_2Ta C14 and C15 Laves phases shown in the secondary phase. The structure of Cr_2Ta refers to Mann's work[1]. To ensure model generality and sufficient data diversity, the RMEA structure was applied with a scaling factor range of 0.97 to 1.03 for uniform lattice deformation.

During the exploration stage, long-time MD simulation was conducted using one of four potentials, following which the remaining three potentials were utilised to predict the associated energies and atomic forces, whereas a maximum force deviation, σ_f^{max}, for MD-simulated configurations under four potentials can be obtained. The accurate configuration was defined as the σ_f^{max} was less than the set minimum force error, σ_{low}. A convergence criterion of iteration was ruled as the percentage of accurate configurations exceeding 99%[2,3]. While the iteration was not converged, meaning the potential was not accurate enough, configurations in the MD simulation would be added to the training dataset based on their σ_f^{max} and criteria value of lower bounds σ_{low} and higher bounds σ_{high}. Configurations falling within the range $\sigma_{low} < \sigma_f^{max} < \sigma_{high}$ were labelled as "candidate", which were used for first-principle calculations and added to the dataset. Configurations with $\sigma_f^{max} > \sigma_{high}$ indicated poor model predictions and were labelled as "fail", and these configurations were eliminated.

To cover more configuration space, a wide temperature and pressure range was explored, and different model deviation MD task iteration was conducted on the above structure. Three temperature ranges were explored, including room temperature or low temperature (LT) range [50 K, 100 K, 150 K, 200 K, 300 K, 400 K], medium temperature (MT) range [0.2, 0.3, 0.4, 0.5, 0.6, 0.7]T_m (The melting point, T_m = 2,580 K, was calculated based on the average rule of those of four elements), and high temperature (HT) range [0.8, 0.9, 1.0, 1.1, 1.2, 1.3]T_m. The DPGEN exploration process included the exploration in room temperature, medium temperature, and high-temperature range in an isothermal-isobaric (NpT) ensemble. Moreover, a canonical (NVT) ensemble at room temperature was also simulated to explore the interaction of atoms for surface behaviour. The lower bound and upper bound change according to the temperature range, that for room temperature was [0.12, 0.25], for medium temperature was [0.20, 0.35] and for high temperature was [0.25, 0.40]. Model deviation MD tasks included default model deviation MD from DPGEN, Monte Carlo MD (MCMD) calculation, and tensile MD simulation. The MCMD simulation incorporates atom displacements and the exchange of atom types within pairs to facilitate the exploration of a broader spectrum of potential random structures. On the other hand, tensile MD can emulate the tensile process, providing insights into various mechanical properties of the system.

1.3 DFT Calculation Setting

No additional information for the DFT calculation setting.

1.4 DPMD Calculation Setting

The equilibrium properties, including lattice constants, elastic matrix constants (C_{11}, C_{12} and C_{44}), mechanical modulus (bulk, shear and Young's modulus), Poisson's ratio, and micro-hardness, were analysed. The lattice constant was determined using the Birch–Murnaghan equation[4] to establish the relationship between energy and lattice constant, ranging from 2.8 to 3.4. The elastic matrix constants were determined using the explicit deformation method, where an equilibrium stress tensor was obtained with a small deformation in each direction[5]. Following the derivation of the elastic matrix constants, a series of mechanical properties, including bulk modulus, shear modulus, Young's modulus, and hardness, was calculated using the Voigt-Reuss-Hill (VRH) approximation as detailed in **Equation S2-3** in the Supplementary Information[6,7]. Additionally, the Vickers hardness was computed by $Hv = \frac{(1-2v)B}{6(1+v)}$ [8], which exhibited good predictability for metal materials with a density exceeding 4 g/cm^3 [9].

The structural properties of RMEA were investigated by the total radial distribution function (RDF), g(r). The 128-atom SQS structure was equilibrated for 100 ps. Then, from 300 K to 3,300 K with a step of 500 K, the structure of RMEA was recorded at each temperature for 100 ps, yielding a total of 100 frames. The temperature was increased to the next level within 50 ps. The coordination analysis function in OVITO was applied to calculate the average RDF curve of the last 10 frames[10].

2 Empirical equations for mechanical properties

After obtaining the elastic matrix constant, various mechanical properties could be calculated using the Voigt-Reuss-Hill (VRH) approximation[6,7], including bulk modulus B, Young's modulus E, shear modulus G, and Poisson's ratio v:

$$\mathrm{B} = \frac{\mathrm{B_V}+\mathrm{G_R}}{2}\ ;\ \mathrm{G} = \frac{\mathrm{G_V}+\mathrm{G_R}}{2};\ \mathrm{E} = \frac{9\mathrm{BG}}{3\mathrm{B}+\mathrm{G}};\ \mathrm{v} = \frac{3\mathrm{B}-\mathrm{E}}{6\mathrm{B}} \qquad \textbf{Equation S2}$$

In which Voigt and Reuss's bounds represent the lower and upper limits of bulk modulus and shear modulus. The Voigt and Reuss bounds for bulk modulus B and shear modulus G can be given by[7,11]:

$$B_V = B_R = \frac{1}{3}(C_{11} + 2C_{12})$$

$$G_V = \frac{1}{5}(C_{11} - C_{12} + 3C_{44})$$

$$G_R = \frac{5 \cdot (C_{11} - C_{12}) \cdot C_{44}}{4 \cdot C_{44} + 3(C_{11} - C_{12})}$$ **Equation S3**

Supplementary Figures

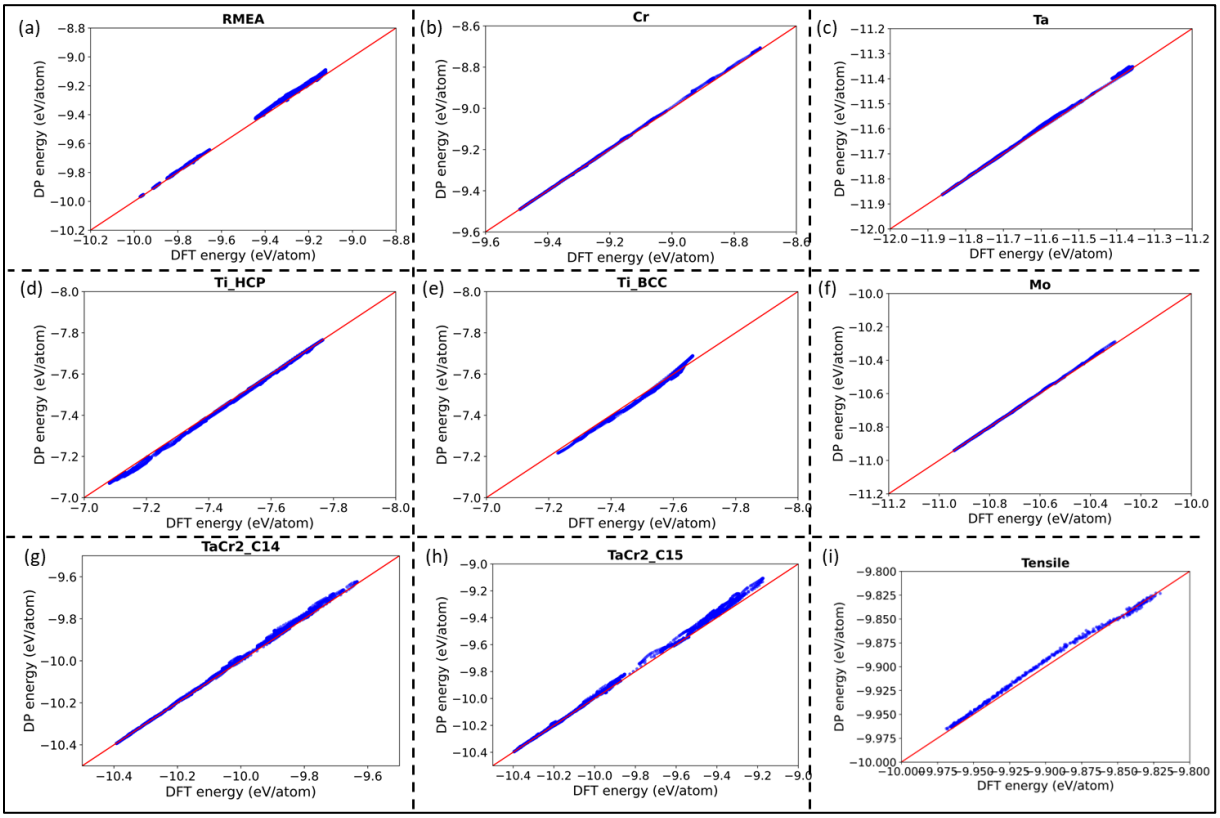

Fig. S1. Energy validation of individual dataset. (a) RMEA, (b) Cr, (c) Ta, (d) Ti_HCP, (e) Ti_BCC, (f) Mo, (g) TaCr2_C14, (h) TaCr2_C15, (i) Tensile.

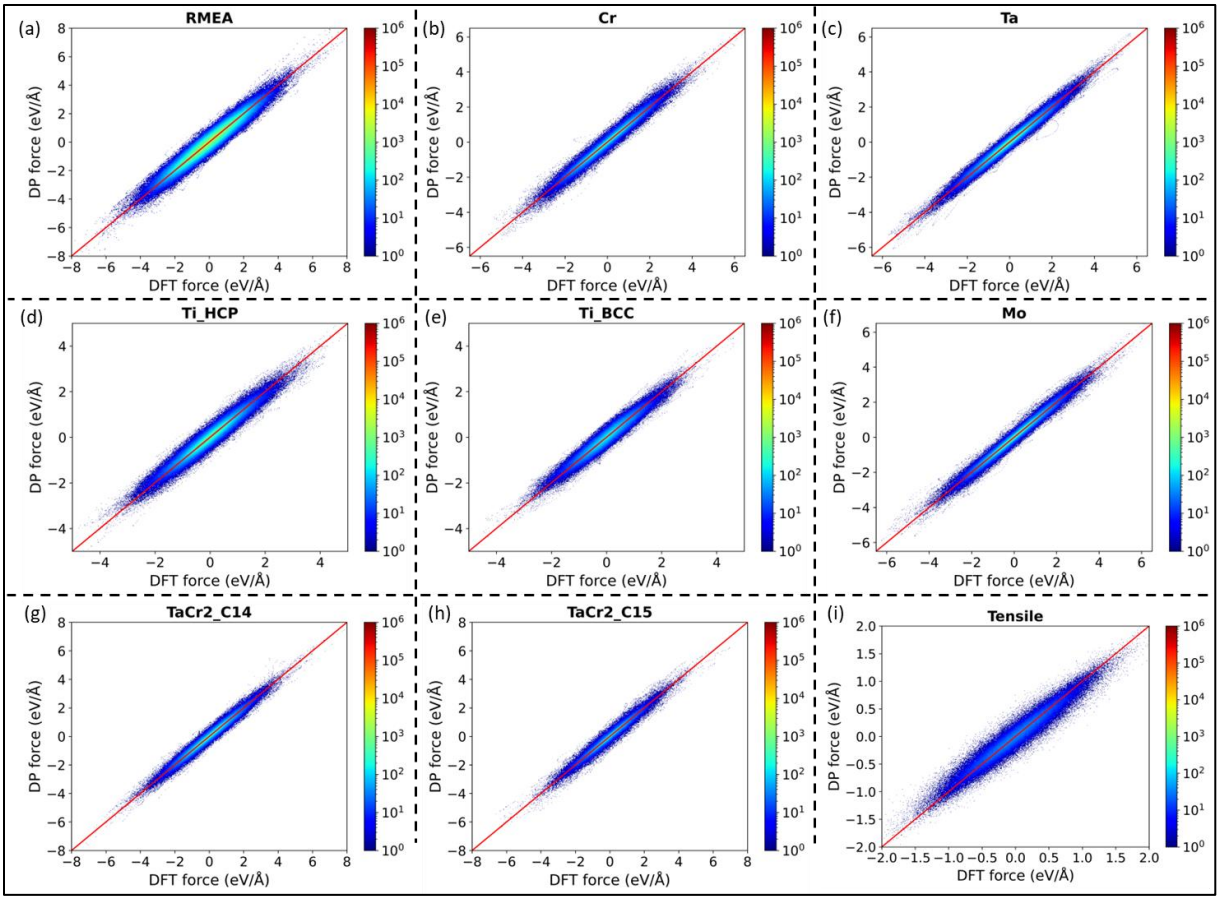

Fig. S2. Force validation of individual dataset. (a) RMEA, (b) Cr, (c) Ta, (d) Ti_HCP, (e) Ti_BCC, (f) Mo, (g) TaCr2_C14, (h) TaCr2_C15, (i) Tensile.

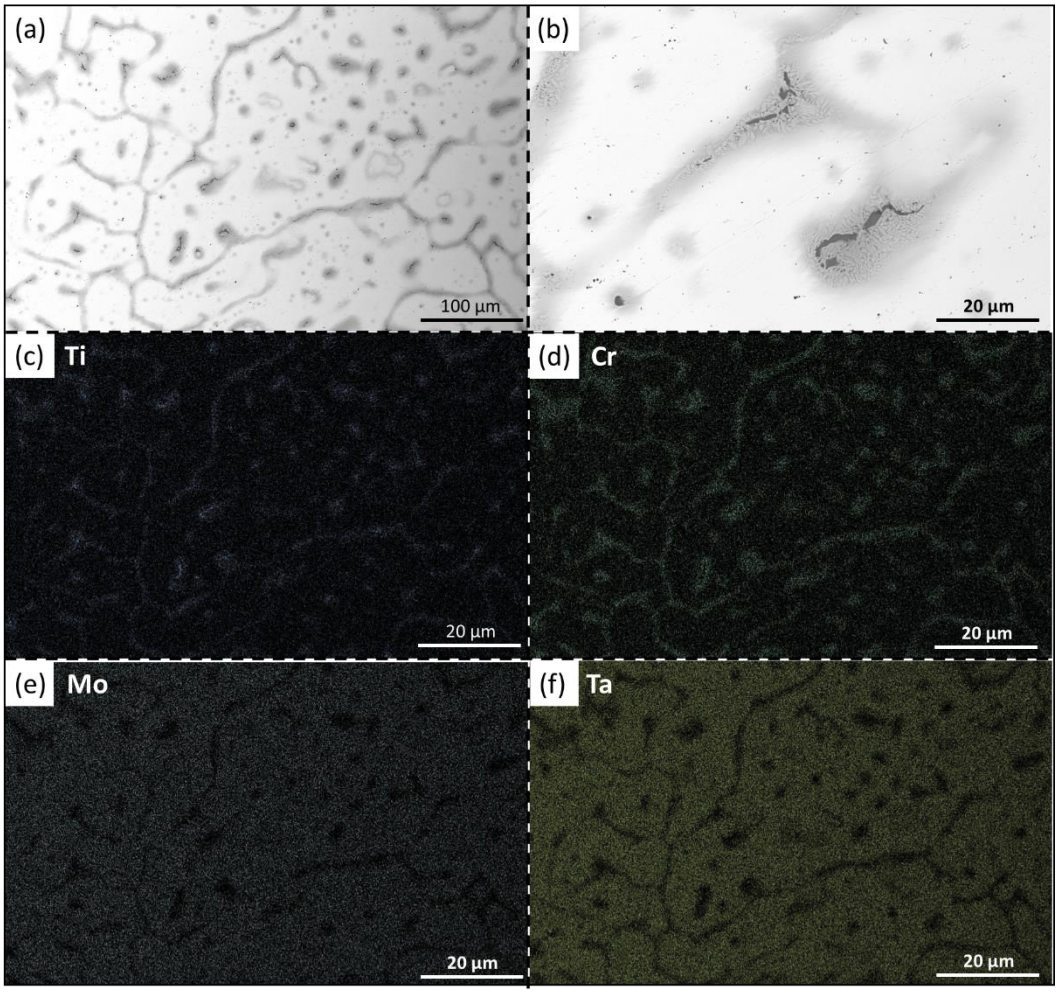

Fig. S3. The SEM/EDS results of the as-cast CrTaTiMo RMEA. SEM photo under (a) 1000× magnification, and (b) 5000× magnification. EDS photo under 5000× magnification of (a) Ti, (b) Cr, (c) Mo, and (d) Ta.

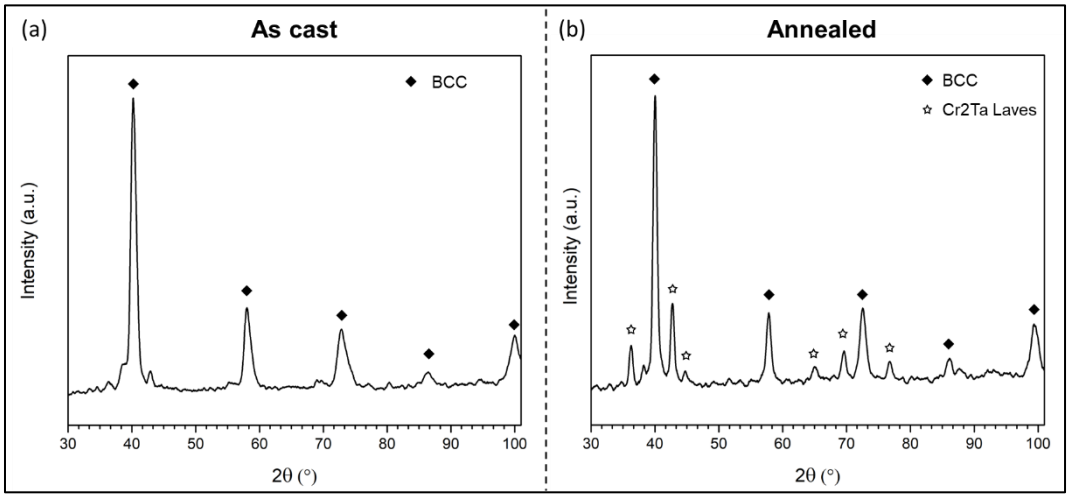

Fig. S4. XRD figure of the CrTaTiMo RMEA, (a) as-cast, (b) annealed.

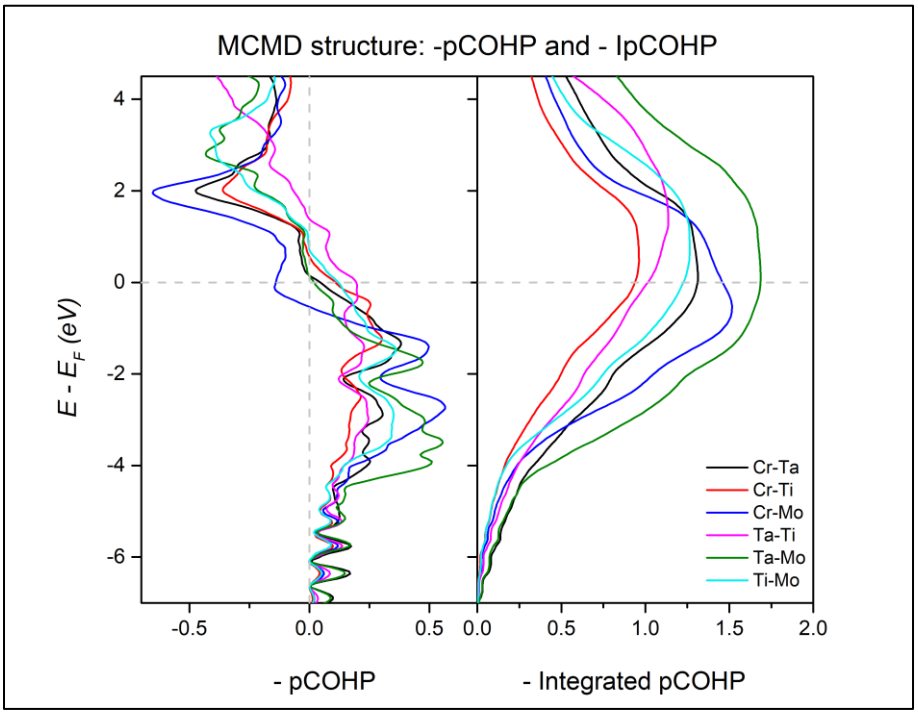

Fig. S5. pCOHP and Integrated pCOHP in 128-atom MCMD structure.

Supplementary Tables

Table S1. Exploration setting of DPGEN iterations.

Structure & System	Iteration	Length (ps)	Accurate (%)	Candidate (%)	Failed (%)	Added data	Criteria for maximum force error [lo, hi]
1. Low T (LT). RMEA (128 atoms). NpT.	Iter.00	1	80.7	19.4	0	180	[0.05, 0.20]
	Iter.01	3	85.5	14.5	0	180	
	Iter.02	6	88.5	11.6	0	180	
	Iter.03	12	90.8	9.2	0.1	180	
	Iter.04	25	99.95	0.05	0	0	[0.10, 0.25]
	Total					**720**	
2. LT. RMEA, MCMD. NpT.	Iter.05	1	2.0	31.7	66.3	180	
	Iter.06	3	30.9	65.4	3.8	180	
	Iter.07	6	99.2	0.8	0	34	
	Total					**394**	
3. LT. RMEA, Tensile MD (3%, 8%, 15%). NpT.	Iter.08	3	98.1	1.9	0	60	
	Iter.09	8	98.5	1.5	0	60	
	Iter.10	15	83.6	15.9	0.5	141	
	Iter.11	15	96.7	3.3	0	142	
	Iter.12	15	98.6	1.5	0	151	
	Iter.13	15	98.5	1.5	0	109	
	Iter.14	15	99.3	0.7	0	11	[0.12, 0.25]
	Total					**674**	
4. LT. Pure element. Cr, Mo, Ta, bcc (128, respectively); Ti_hcp (96). NpT.	Iter.15	1	4.1	51.9	44.1	240	
	Iter.16	3	83.1	14.1	17.7	125	
	Iter.17	6	95.2	4.8	0	100	
	Iter.18	12	100.0	0.0	0	0	
	Total					**465**	
6. LT. Cr_2Ta. C14 (48) & C15 (24). NpT.	Iter.23	1	54.8	45.2	0.1	200	
	Iter.24	3	94.3	5.7	0.1	148	
	Iter.25	6	99.9	0.0	0.0	0	
	Iter.26	12	100.0	0.0	0.0	0	
	Iter.27	25	100.0	0.0	0.0	0	
	Total					**348**	
7. Medium T (MT). RMEA. NpT.	Iter.28	1	37.9	47.5	14.6	300	[0.15, 0.30]
	Iter.29	3	29.9	60.6	7.1	227	
	Iter.30	6	73.6	25.4	1.0	229	
	Iter.31	12	80.2	19.5	0.3	237	
	Iter.32	25	82.7	18.9	0.2	236	
	Iter.33	40	89.1	10.8	0.1	239	
	Iter.34	60	88.6	11.4	0.1	234	
	Iter.35	80	2.2	74.7	24.7	240	[0.20, 0.35]
	Iter.36	100	99.1	0.9	0.0	0	

	Iter.37	120	99.6	0.4	0.0	0	
	Total					**1,942**	
8. MT. RMEA, MCMD. NpT.	Iter.38	1	99.3	0.7	0.0	33	
	Iter.39	3	99.3	0.7	0.0	0	
	Iter.40	6	99.3	0.7	0.0	0	
	Iter.41	12	99.1	0.9	0.0	16	
	Total					**49**	
9. MT. Pure element, Cr_2Ta. Cr, Mo, Ta, Ti (128), bcc; Ti_hcp. Cr2Ta, C14&C15. NpT.	Iter.42	0.5	93.3	6.2	0.5	380	
	Iter.43	1	91.3	8.4	0.2	280	
	Iter.44	3	99.8	0.2	0.0	0	
	Iter.45	6	99.8	0.2	0.0	0	
	Iter.46	12	99.8	0.2	0.0	0	
	Iter.47	25	99.8	0.2	0.0	0	
	Total					**660**	
10. High T (HT). RMEA. NpT.	Iter.48	1	60.5	30.6	8.9	240	
	Iter.49	3	63.7	30.8	5.5	240	
	Iter.50	6	79.9	18.4	1.7	240	
	Iter.51	12	88.2	11.1	0.8	240	
	Iter.52	25	94.3	5.3	0.3	240	
	Iter.53	40	96.0	3.9	0.1	190	
	Iter.54	60	97.6	2.4	0.1	107	
	Iter.55	80	97.2	3.8	0.1	138	
	Iter.56	100	97.9	2.0	0.1	111	
	Iter.57	120	99.3	0.7	0.0	0	[0.23,0.38]
	Total					**1,746**	
11. HT, RMEA, MCMD, NpT.	Iter.58	1	99.4	0.6	0.0	19	
	Iter.59	3	99.3	0.7	0.0	18	
	Iter.60	6	99.1	0.8	0.0	34	
	Iter.61	12	99.2	0.8	0.0	23	
	Iter.62	25	99.5	0.5	0.0	0	
	Total					**94**	
12. HT. Pure element, Cr_2Ta. Cr, Mo, Ta, Ti, bcc; Ti_hcp. Cr_2Ta, C14&C15. NpT.	Iter.63	1	96.87	1.78	0.23	160	
	Iter.64	3	98.77	0.70	0.09	92	
	Iter.65	6	99.22	0.42	0.08	32	
	Iter.66	12	98.78	0.73	0.06	80	
	Iter.67	25	99.41	0.37	0.01	42	
	Iter.68	40	99.47	0.32	0.02	21	
	Iter.69	60	99.51	0.29	0.03	0	
	Total					**427**	
13. LT. RMEA, NVT.	Iter.70	1	89.40	10.60	0.00	36	[0.10, 0.25]
	Iter.71	3	92.52	5.37	0.00	35	
	Iter.72	6	96.62	3.38	0.00	0	
	Iter.73	12	96.51	3.49	0.00	29	
	Iter.74	25	97.49	2.51	0.00	0	
	Iter.75	40	98.40	1.60	0.00	0	
	Iter.76	60	98.33	1.67	0.00	0	
	Iter.77	80	100.00	0.00	0.00	0	[0.12, 0.25]

	Total					**100**	
14. LT. Cr, Mo, Ta, Ti, bcc; Ti_hcp. Cr_2Ta, C14&C15. NVT.	Iter.78	1	100.00	0.00	0.00	0	
	Iter.79	6	100.00	0.00	0.00	0	
	Iter.80	25	100.00	0.00	0.00	0	
	Total					**0**	
2*. LT. RMEA, MCMD. NpT.	Iter.81	1	98.87	1.13	0.00	62	[0.10, 0.25]
	Iter.82	3	97.73	2.27	0.00	125	
	Iter.83	6	89.41	10.59	0.00	233	
	Iter.84	12	99.18	0.82	0.00	32	
	Iter.85	25	99.05	0.95	0.00	48	
	Iter.86	40	93.22	6.78	0.00	225	
	Iter.87	60	99.96	0.04	0.00	0	
	Iter.88	80	99.93	0.07	0.00	0	
	Iter.89	80	99.89	0.11	0.00	0	
	Total					**725**	

PS:
1. The author considered training the PD and SI phase structure data. However, due to the unpredictable atomic composition in these two phases at the beginning of the potential training stage, the initial PD and SI phase structure used for potential training did not align well with the chemical composition in the latest EDS experimental results. In this way, the iteration about PD and SI phase structure was deleted, such as Stage 5, iter 19-22, etc.
2. The atom number in each configuration is listed in brackets, such as "Cr, Mo, Ta, bcc (128, respectively)", representing that the configurations for Cr, Mo, and Ta elements have 128 atoms, respectively. Without marking, the configurations used in later iterations are the same as the previous configuration.
3. The criteria for maximum force error for each temperature range were adjusted. The final criteria are: LT, [0.12, 0.25]; MT, [0.20, 0.35]; HT, [0.23, 0.38].

Table S2. RMSE for all structures in the validation dataset of the CrTaTiMo RMEA.

Structure	RMSE-Energy (meV/atom)	RMSE-Force (eV/Å)
RMEA	15.72	0.244
Cr	4.65	0.156
Ta	6.19	0.154
Ti_HCP	10.43	0.179
Ti_BCC	15.31	0.188
Mo	4.44	0.150
Tensile	4.46	0.125
Cr_2Ta_L14	9.35	0.180
Cr_2Ta_L15	20.64	0.202

Table S3. The interaction between different element pairs within the SQS and the SRO structure.

Pair	SQS	SRO
Cr-Ta	68	120
Cr-Ti	70	102
Cr-Mo	65	22
Ta-Ti	70	28
Ta-Mo	65	111
Ti-Mo	68	85
Total	406	468

Supplementary Reference

1 Mann, A. E. & Newkirk, J. W. Compositional Modifications to Alter and Suppress Laves Phases in AlCrMoTaTi Alloys. *Advanced Engineering Materials* **25**, 2201614 (2023). https://doi.org:https://doi.org/10.1002/adem.202201614

2 He, R. *et al.* Structural phase transitions in SrTiO3 from deep potential molecular dynamics. *Physical Review B* **105**, 064104 (2022). https://doi.org:10.1103/PhysRevB.105.064104

3 Zhao, J., Feng, T. & Lu, G. Atomistic simulations on liquid Mg–Sr alloys assisted with deep learning potential. *Journal of Materials Science* **59**, 13558-13574 (2024). https://doi.org:10.1007/s10853-024-09937-2

4 Birch, F. Finite Elastic Strain of Cubic Crystals. *Physical Review* **71**, 809-824 (1947). https://doi.org:10.1103/PhysRev.71.809

5 Clavier, G. *et al.* Computation of elastic constants of solids using molecular simulation: comparison of constant volume and constant pressure ensemble methods. *Molecular Simulation* **43**, 1413-1422 (2017). https://doi.org:10.1080/08927022.2017.1313418

6 Yao, H., Ouyang, L. & Ching, W.-Y. Ab Initio Calculation of Elastic Constants of Ceramic Crystals. *Journal of the American Ceramic Society* **90**, 3194-3204 (2007). https://doi.org:https://doi.org/10.1111/j.1551-2916.2007.01931.x

7 Wu, Z.-j. *et al.* Crystal structures and elastic properties of superhard IrN2 and IrN3 from first principles. *Physical Review B* **76**, 054115 (2007). https://doi.org:10.1103/PhysRevB.76.054115

8 Miao, N., Sa, B., Zhou, J. & Sun, Z. Theoretical investigation on the transition-metal borides with Ta3B4-type structure: A class of hard and refractory materials. *Computational Materials Science* **50**, 1559-1566 (2011). https://doi.org:https://doi.org/10.1016/j.commatsci.2010.12.015

9 Dovale-Farelo, V., Tavadze, P., Lang, L., Bautista-Hernandez, A. & Romero, A. H. Vickers hardness prediction from machine learning methods. *Scientific Reports* **12**, 22475 (2022). https://doi.org:10.1038/s41598-022-26729-3

10 Stukowski, A. Visualization and analysis of atomistic simulation data with OVITO–the Open Visualization Tool. *Modelling and Simulation in Materials Science and Engineering* **18**, 015012 (2010). https://doi.org:10.1088/0965-0393/18/1/015012

11 Zhao, Q., Li, J., Fang, Q. & Feng, H. Effect of Al solute concentration on mechanical properties of AlxFeCuCrNi high-entropy alloys: A first-principles study. *Physica B: Condensed Matter* **566**, 30-37 (2019). https://doi.org:https://doi.org/10.1016/j.physb.2019.04.025